Acta Crystallographica Section D
Biological Crystallography
ISSN 0907-4449

The structure of mouse tumour-necrosis factor at 1.4 Å resolution: towards modulation of its selectivity and trimerization

K. J. Baeyens,[a] H. L. De Bondt,[a] A. Raeymaekers,[b] W. Fiers[b] and C. J. De Ranter[a]*

[a]Laboratorium voor Analytische Chemie en Medicinale Fysicochemie, E. Van Evenstraat 4, B-3000 Leuven, Belgium, and [b]Laboratorium voor Moleculaire Biologie, Universiteit Gent, Ledeganckstraat 35, B-9000 Gent, Belgium

Correspondence e-mail: camiel.deranter@farm.kuleuven.ac.be

Received 7 October 1998
Accepted 24 December 1998

PDB Reference: mouse tumour-necrosis factor, 2tnf.

The 1.4 Å resolution structure of recombinant mouse tumour-necrosis factor α (mTNF) at 100 K has been determined. The crystals are triclinic, space group $P1$, with unit-cell parameters $a = 48.06$, $b = 48.18$, $c = 51.01$ Å, $\alpha = 114.8$, $\beta = 103.6$, $\gamma = 91.1^\circ$. The structure was refined to a final crystallographic R value of 19.7% ($R_{\rm free}$ = 23.3%), including 3477 protein atoms, one 2-propanol molecule, one Tris molecule and 240 water molecules. Throughout the crystal lattice, the trimers are differently packed compared with human TNF, which was crystallized in the tetragonal space group $P4_12_12$ and refined to 2.6 Å resolution. The structures of mTNF and human TNF are very similar, diverging mainly in regions that are either flexible and/or involved in crystal packing. Some loops in mTNF which contain residues important for receptor binding are better resolved than in human TNF, such as the surface-exposed loops 30–34 and 144–147, which are also important for receptor specificity. Compared with human TNFs, the channel formed by the three monomers in mTNF is narrower. One 2-propanol molecule trapped in the trimeric channel could be a lead compound for the design of TNF inhibitors.

1. Introduction

Tumour-necrosis factor α (TNF) belongs to the cytokine family of polypeptide mediators, a group which includes the interferons and the interleukins. TNF is an important mediator in inflammation, immune responses (Vassalli, 1992; Fiers, 1995) and infection-related phenomena (Vassalli, 1992), but prolonged overexpression leads to severe toxicity, which limits the use of TNF as an anticancer agent. TNF, a trimer of 17.35 kDa subunits, exerts its diverse biological properties by binding to and clustering distinct cell-surface receptors of 55 kDa (TNF receptor 1 or TNF-R55) and 75 kDa (TNF receptor 2 or TNF-R75) (Vandenabeele *et al.*, 1995), both members of the large TNF-receptor superfamily. Cellular signalling occurs by triggering one or both of the receptors depending on the cell type and condition. It is known that one TNF trimer binds to three TNF receptors and that the binding occurs in the groove region between each pair of subunits in the trimer (Eck & Sprang, 1989; Van Ostade *et al.*, 1991), as shown in the crystal structure of tumour-necrosis factor β (lymphotoxin) with the extracellular domain of TNF-R55 (Banner *et al.*, 1993). Furthermore, site-directed mutagenesis studies have shown that the residues crucial for receptor binding and biological activity are located in the intersubunit grooves of the tumour-necrosis factor α (TNF) trimer (Yamagishi *et al.*, 1990; Van Ostade *et al.*, 1991; Zhang *et al.*, 1992).

Remarkably, human TNF binds to murine TNF-R55 but not to TNF-R75 (Vandenabeele *et al.*, 1995). This allows uncoupling of the TNF-R55- and TNF-R75-mediated activities in the mouse. Interestingly, *in vivo* toxicity of human TNF in normal mice was found to be approximately 50 times lower than mouse TNF, while selective tumour toxicity remained unaffected (Brouckaert *et al.*, 1992), suggesting a special role for TNF-R75 in TNF-induced systemic toxicity. Since in the human system the TNF-R55-specific mutants L29S, R32W and E146K could act as the equivalent of human TNF in mice, they offer the prospect of reduced general cytotoxicity when used in cancer patients (Van Ostade *et al.*, 1993; Barbara *et al.*, 1994). Uncoupling of TNF-R55- and TNF-R75-mediated activities is also possible in the mouse system using appropriately mutated mouse TNF (Ameloot *et al.*, in preparation). This offers the possibility of testing the efficacy of differentially binding muteins *in vivo* in mice, since these mouse TNF mutants are expected to be almost non-immunogenic, in contrast to human TNF. The questions of why mouse TNF binds to both human TNF receptors and why human TNF binds only to mouse TNF-R55 need to be solved in order to fully understand what exactly is required for development of TNF-R55 specific human TNF analogues.

2. Materials and methods

2.1. Sample preparation and crystallization

The preparation of recombinant mouse TNF and its crystallization have been described previously (Baeyens *et al.*, 1997). Single crystals were obtained by the sitting-drop vapour-diffusion method at 277 K from droplets consisting of equal volumes of reservoir solution (containing 7% 2-propanol, 30% MEPEG 2000, 0.1 *M* Tris buffer at pH 8.5) and protein solution (containing 0.5% NaCl, 11 mg ml^{-1} protein, 10 m*M* HEPES buffer at pH 6.8). The crystals belong to the triclinic space group *P*1 with unit-cell parameters $a = 48.06$, $b = 48.18$, $c = 51.01$ Å, $\alpha = 114.8$, $\beta = 103.6$, $\gamma = 91.1^\circ$.

```
TNF     1           10          20          30          40
mouse   LRSSSQNSSD  KPVAHVVANH  QVEEQLEWLS  QRANALLANG
human   VRSSSRTPSD  KPVAHVVANP  QAEGQLQWLN  RRANALLANG
                      EEEEEE        EE        EEE

TNF                50          60          70          80
mouse   MDLKDNQLVV  PADGLYLVYS  QVLFKGQGCP  DY-VLLTHTV
human   VELRDNQLVV  PSEGLYLIYS  QVLFKGQGCP  STHVLLTHTI
          EEE   EEE     EEEEEEE  EEEEEEE        EEEEE

TNF                90          100         110         120
mouse   SRFAISYQEK  VNLLSAVKSP  CPKDTPEGAE  LKPWYEPIYL
human   SRIAVSYQTK  VNLLSAIKSP  CQRETPEGAE  AKPWYEPIYL
        EEE       E  EEEEEEEE                EEEEEEEE

TNF              130         140         150       157
mouse   GGVFQLEKGD  QLSAEVNLPK  YLDFAESGQV  YFGVIAL
human   GGVFQLEKGD  RLSAEINRPD  YLDFAESGQV  YFGIIAL
        EEEEEE      EEEEEE GGG G            EEEEEE
```

Figure 1
Sequence alignment of mTNF against human TNF along with the secondary-structure assignment according to *PROMOTIF* (Hutchinson & Thornton, 1996). Sequence differences are printed in bold.

2.2. Data collection and processing

The X-ray diffraction data were collected from a single crystal under cryogenic conditions (at approximately 100 K). The mother liquor served as the cryoprotectant and a crystal of dimensions 0.25 × 0.25 × 0.20 mm was mounted in a nylon loop and flash-frozen in liquid nitrogen.

X-ray diffraction data were collected at DESY/EMBL (Hamburg) using a MAR image-plate detector (30 cm) and synchrotron radiation of wavelength 1.1024 Å (beamline BW7B). Data to 1.38 Å were recorded. The data were collected in images corresponding to 1.3° rotations and a crystal-to-detector distance of 140 mm. A total of 140 images resulted in 72552 unique reflections from 128698 observations with an $R_{\rm merge}$ of 2.9%. The data were integrated and scaled using the programs *DENZO* and *SCALEPACK* (Otwinowski, 1993).

2.3. Phasing and model building

The structure was solved by the molecular-replacement method using the program *X-PLOR* 3.1 (Brünger, 1992*a*). *X-PLOR* version 3.843 was used for the refinement. As the amino-acid sequences of mouse TNF and human TNF are 79% identical, the atomic coordinates of human TNF (accession number 1TNF in the Protein Data Bank) were used as a search model (Eck & Sprang, 1989; Jones *et al.*, 1989). A sequence alignment of mTNF against human TNF, along with the secondary-structure assignment, is shown in Fig. 1. A self-rotation search confirmed the presence of a trimer with non-crystallographic symmetry. For the initial calculation of the rotation function, the trimer from the model was used. The molecular-replacement method based on Patterson correlation (PC) refinement (Brünger, 1990) gave a clear solution in the resolution range 15–4 Å, with PC coefficients of 0.93, 0.89 and 0.86 for the first three peaks of the cross-rotation function; the PC coefficient for the highest background peak was 0.46. No translation search was performed as the crystals belong to space group *P*1 and the origin could therefore be chosen to be anywhere.

10% of the reflections (7076) were used for the free *R*-factor calculation (Brünger, 1992*b*). After one cycle of rigid-body refinement and 300 cycles of Powell minimalization, the *R* factor and $R_{\rm free}$ were 32.3 and 47.7%, respectively, in the resolution range 8.0–2.5 Å. The non-glycine residues (33 amino acids) which differ from human TNF were replaced in the model by alanine. Simulated annealing (Brünger *et al.*, 1987, 1990) was performed, starting from a temperature of 3000 K and slowly cooling in decreasing steps of 25 K to 300 K. The geometry was restrained using the parameter file

Table 1
Data collection and refinement statistics for mouse TNF.

Unit-cell parameters (Å, °)	a = 48.06, b = 48.18, c = 51.01, α = 114.8, β = 103.6, γ = 91.1
Space group	$P1$
Resolution range (Å)	8.0–1.40
Number of reflections	
Total (no cutoff)	128698
Unique	72552
Used for refinement (working/test) [$2\sigma(F)$ cutoff]	63692/7076
Mosaicity (°)	0.9
$R_{\rm merge}$† (%)	
Overall	2.9
1.5–1.4 Å	14.8
Redundancy	1.77
Completeness (%)	
Overall	90.9
1.5–1.4 Å	85.5
Initial R factor (8–2.5 Å) (%)	32.3
Initial $R_{\rm free}$ factor (8–2.5 Å) (%)	47.6
Final R factor (8–1.4 Å) (%)	19.7
Final $R_{\rm free}$ factor (8–1.4 Å) (%)	23.3
Refined model	
Protein atoms	3477
Water molecules	240
2-Propanol molecule	1
Tris molecule	1
Parameter file	parhcsdx.pro
Topology file	tophcsdx.pro
R.m.s. deviation of the model	
Bond lengths (Å)	0.014
Bond angles (°)	1.86
Dihedral angles (°)	27.5
Improper angles (°)	1.60
Average atomic temperature factors of the refined model (Å^2)	
Main chain	18.6
Side chain	20.5
Water molecules	21.8
2-Propanol and Tris	18.2

† $R_{\rm merge} = \sum|I - \langle I\rangle|/\sum I$.

of Engh & Huber (1991). Bulk-solvent corrections (Jiang & Brünger, 1994) were always applied. Each round of refinement was alternated with a round of manual refitting using the program *O* (Jones *et al.*, 1991) on Silicon Graphics workstations. Difference omit electron-density maps were always used in model rebuilding.

In order to avoid averaging out the individual differences between the three monomers and given the high number of observations, non-crystallographic symmetry restraints were not used. The resolution was slowly increased from 2.5 to 2.1 Å. At this point grouped B factors were refined. A search for water molecules was then initiated. Water molecules were included in the refinement only when the following criteria were met: (i) a well shaped peak was present at a cutoff of 4.0σ in the $F_o - F_c$ maps and $2F_o - F_c$ electron-density maps, (ii) the peak was surrounded by at least one proton acceptor/donor partner and (iii) the final B value was less than 37 Å^2. The highest peaks turned out to be a 2-propanol and a Tris molecule. The resolution was further increased to a final resolution of 1.4 Å. Restrained individual isotropic temperature factors were refined for all non-H atoms from resolution 1.7 Å onwards. The final model lacks residues 1–8 at the N-terminus. The electron density is poor for residues 103–107 in subunits A and C which are part of a very flexible loop with high B factors. The final model consists of 444 residues, one 2-propanol molecule, one Tris molecule and 240 water molecules. A portion of the final $2F_o - F_c$ electron-density map is shown in Fig. 2.

The final values of $R_{\rm cryst}$ and $R_{\rm free}$ are 19.7 and 23.3%, respectively. The model is of excellent quality and consistent with other structures of its size and resolution according to the program *PROCHECK* (Laskowski *et al.*, 1993). The crystallographic parameters are summarized in Table 1.

3. Results and discussion

3.1. The overall structure

The estimated coordinate error of the model is 0.17 Å (Luzzati, 1952). The model has good geometry, with 99.5% of residues in the most preferred regions in the Ramachandran plot (Fig. 3). Three residues are located in generously allowed regions. These residues belong to flexible loops and have poor electron density. The structure of an mTNF monomer, which consists of 156 residues, folds into a 'jelly roll' (a β-sheet sandwich consisting almost entirely of antiparallel β-strands) and forms a bell-shaped rigid trimeric molecule with two other subunits. As a result, a channel is formed along the trimer axis (trimeric channel), lined by charged and polar residues near the top and the bottom and by hydrophobic residues in the middle part. As expected, the exterior surface is composed mostly of charged and polar residues. The only cysteine bridge in each TNF monomer is localized

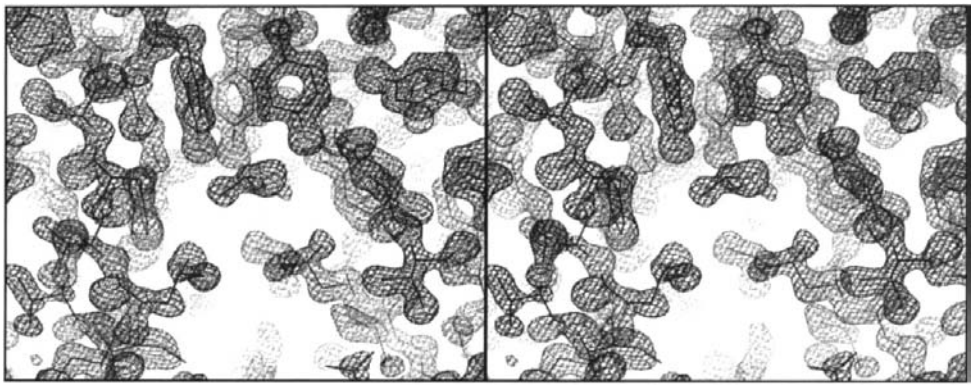

Figure 2
A stereoview of a portion of the final ($2F_o - F_c$) electron-density map at 1.4 Å (contoured at 1.0σ) with the refined model superimposed. The threefold axis lies vertical. The three tyrosine side chains of residues 119 of subunits A, B and C are related by this threefold. The 2-propanol molecule, in the centre of the picture, lies approximately on this threefold axis.

near the top, while the N- and C-termini are located at the bottom of the structure.

The average *B* values of the main chain, the side chain, the 2-propanol and Tris molecules, and the water molecules together with some root-mean-square (r.m.s.) deviations for the model are given in Table 1. Not surprisingly, the *B* factors are highest at the N-terminus and in some loop regions. The *B* factors are also similar in the three subunits, despite their different crystal contacts.

It is known that TNF is relatively resistant to organic solvents (Aggarwal, 1990; Porter, 1990). Interestingly, mTNF was crystallized in the presence of 7% 2-propanol and a 2-propanol molecule is located just beneath the ring formed by the Tyr119 residues of the three subunits. A Tris molecule is located just above the ring formed by the Tyr119 residues of the three subunits. The annulus of Tyr119 residues constitutes the closest contact among the three subunits. The OH group of 2-propanol is stabilized by forming two hydrogen bonds of 3.1 Å with Tyr119 OH of subunits *B* and *C*. A C^{α} tracing of the superimposed trimer structures together with the 2-propanol molecule is shown in Fig. 4. The three OH groups of the Tris molecule make hydrogen bonds of 3.0 Å with the peptide bond of residues 119 of subunits *A*, *B* and *C* and three hydrogen bonds of 2.7 Å with ordered water molecules.

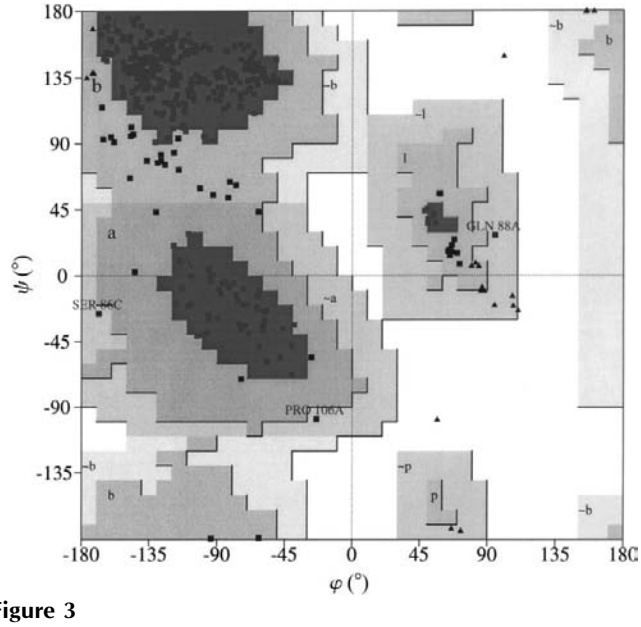

Figure 3
Ramachandran plot calculated using *PROCHECK* (Laskowski *et al.*, 1993). Glycine residues are shown as triangles and the other residues as squares. Residues with conformational angles outside allowed regions are labelled.

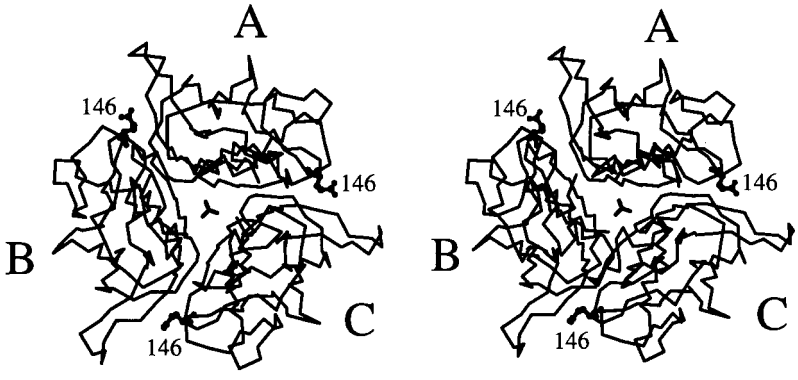

Figure 4
Stereoview of the C^{α} trace of the mTNF trimer looking down into the trimeric channel. One 2-propanol molecule is located in the middle of the channel. The side chain of Glu146 is shown in bold.

3.2. Comparison with human TNF structures

The 1.4 Å mouse TNF structure has the highest resolution of all known TNF structures.

The crystal structure of human TNF has been determined (Jones *et al.*, 1989; Eck & Sprang, 1989) to 2.6 Å. Another structure of human TNF and the R31D mutant have been determined by Weber and co-workers (Reed *et al.*, 1997) to 2.5 and 2.3 Å, respectively. The human TNF M3S mutant has been determined to 1.8 and 2.2 Å (Cha *et al.*, 1998). In the discussion that follows, the structure from Eck & Sprang (1989) will be referred to as 1TNF and the wild-type structure from Reed *et al.* (1997) as hTNF97. The crystals of 1TNF and hTNF97 belong to the same space group, $P4_12_12$, and have the same unit-cell parameters, in contrast to mTNF which belongs to space group *P*1. The superposition of the 1TNF and hTNF97 trimers have an r.m.s. deviation of 0.9 Å for C^{α} atoms. The r.m.s. deviations for C^{α} atoms between the trimer structures of mTNF and 1TNF, and between mTNF and hTNF97 are 1.5 and 1.6 Å, respectively. The subunits within the mTNF trimer differ by an average pairwise r.m.s. deviation (C^{α} atoms) of 1.2 Å. A detailed list of r.m.s. differences is reported in Table 2. Regions 21–26, 30–34, 64–76, 84–91, 99–112 and 138–149 in mTNF are considerably different to human TNFs (Fig. 5). All these regions are mainly located in the loops connecting β-strands. Regions 32–34, 84–91, 117–119 and 143–148 in TNF are critical for biological activity (Yamagishi *et al.*, 1990; Van Ostade *et al.*, 1991). According to site-directed mutagenesis studies, residues 29, 32–35, 84, 86–87, 91, 95, 115, 117, 119, 133, 143 and 146–148 might be involved in receptor binding (Zhang *et al.*, 1992; Van Ostade *et al.*, 1994). Knowing the exact positions of the side chains of these residues might contribute to the understanding of the binding mechanism. The TNF-R75 specific binding region in TNF involves a cluster of three residues, namely Leu29, Arg32 and Glu146 (Van Ostade *et al.*, 1994). Except for loops 84–91 and 99–112, the average *B* factor of mTNF in these loop regions is considerably lower than in human TNFs. An extensive search for symmetry-related contacts showed that in mouse TNF loops 84–91 and 99–112 are not stabilized through symmetry-related contacts, in contrast to human TNFs where these loops are stabilized.

In mTNF, loop region 30–34 is more resolved than in human TNFs. The average *B* factor of C^{α} atoms for residues 30–34 of subunits *A*, *B* and *C* of

Table 2
Comparison of mouse TNF and human TNF structures.

R.m.s. differences: intersubunit pairwise comparisons on C^{α} atoms (Å)

	mTNF	1TNF	hTNF97
A–*B*	1.15	0.78	1.13
A–*C*	1.21	0.87	1.06
B–*C*	1.33	0.83	1.00

R.m.s. differences between trimer structures on C^{α} atoms (Å)

	mTNF–1TNF	mTNF–hTNF97	hTNF97–1TNF
Subunit *A*	1.12	1.27	0.72
Subunit *B*	1.33	1.37	0.76
Subunit *C*	1.72	1.77	0.89
Overall	1.51	1.60	0.88

R.m.s. distances of loop regions on C^{α} atoms (Å)

		mTNF–1TNF	mTNF–hTNF97	hTNF97–1TNF
21–26	*A*	2.08	1.89	0.63
	B	1.70	1.26	0.81
	C	1.36	1.27	0.88
	Average	1.71	1.48	0.78
30–34	*A*	1.47	1.62	1.25
	B	0.80	0.68	0.60
	C	1.23	1.72	1.65
	Average	1.17	1.34	1.17
64–76	*A*	1.23	1.38	0.65
	B	1.55	1.38	0.77
	C	1.66	1.77	0.77
	Average	1.48	1.51	0.72
84–91	*A*	1.14	1.23	0.49
	B	2.86	3.49	1.18
	C	1.57	1.67	1.46
	Average	1.86	2.13	1.04
99–112	*A*	2.26	2.84	1.48
	B	2.80	2.74	1.55
	C	4.13	4.27	1.12
	Average	3.06	3.28	1.39
138–149	*A*	1.05	1.09	0.58
	B	1.21	1.11	0.76
	C	1.75	1.34	1.69
	Average	1.34	1.18	1.01

R.m.s. distances on all atoms (Å)

		mTNF–1TNF	mTNF–hTNF97	hTNF97–1TNF
146–148	*A*	2.67	2.56	0.58
	B	4.10	4.33	0.76
	C	5.03	4.96	1.69
	Average	3.93	3.95	1.01

Mean *B* factor (Å^2) for each subunit

	mTNF	1TNF	hTNF97
Subunit *A*	20.23	28.24	28.57
Subunit *B*	18.18	22.80	27.25
Subunit *C*	20.24	28.12	28.92
Overall	19.69	25.61	28.24

mTNF is 15.1 Å^2, while in 1TNF and hTNF97 the corresponding average *B* factor is 41.8 and 35.1 Å^2, respectively. Asn34 of subunits *A*, *B* and *C* in mTNF forms a hydrogen bond with Arg82 of subunits *C*, *A* and *B*, respectively. The average inter-subunit distance between Asn34 OD1 and Arg82 NH2 is 2.9 Å. In the structure of hTNF97 no such hydrogen bond is present. Only Asn34 from subunit *B* forms a hydrogen bond with Arg82 from subunit *A* in the structure of 1TNF. Arg32 NH2 of subunit *A* and *B* of mTNF forms a salt bridge with Asp71 OD1 of subunits *B* and *C*, respectively, of symmetry-related trimers. Owing to different packing of the subunits in the trimer, there is no formation of a salt bridge for Arg32 of subunit *C*. The hydrogen bond, together with this salt bridge, contribute to the stability of this loop in mTNF. In the human TNFs, no such salt bridge is present. Interestingly, in addition to the site-directed mutagenesis studies, which show that amino acid 32 belongs to the TNF-R75 specific region (Van Ostade *et al.*, 1993, 1994), modelling studies have also predicted that amino acids 31, 32 and 33 are involved in receptor binding (Fu *et al.*, 1995).

Tyr115 N of subunits *A*, *B* and *C* makes a hydrogen bond to Ser99 OG of subunits *C*, *A* and *B*, respectively, with an average bond length of 3.0 Å. There is no hydrogen bond in the hTNF97 structure. 1TNF also shows an identical hydrogen bond of 3.2 Å between residue 115 from subunit *C* and residue 99 from subunit *B*. Interestingly, Tyr115 is implied in receptor binding according to the mutagenesis studies (Zhang *et al.*, 1992; Van Ostade *et al.*, 1994) and the modelling studies of the complex (Fu *et al.*, 1995). Mutation of this core residue results in impaired or reduced receptor binding and cytotoxic activity. This residue and other residues (Trp28, Tyr56, Ser60, His78 and Tyr119) are likely to be important for correct folding of TNF. Mutations of these core residues impaired trimer formation, leading to the loss of biological activity.

The loop region containing residues 146–148 has an average *B* factor of 14.5 Å^2 on C^{α} atoms, while the average *B* factor on C^{α} atoms in 1TNF and hTNF97 is 37.3 and 34.5 Å^2, respectively. The side chain of Glu146 in subunits *A*, *B* and *C* from mTNF points towards the solvent and does not make intermolecular contacts, which makes this residue very accessible for TNF-receptor binding. This confirms the role of Glu146 in receptor binding as had previously been suggested (Van Ostade *et al.*, 1994). This is in contrast to Glu146 from 1TNF and hTNF97, where the side chains of subunits *A*, *B* and *C* are rotated away by 180° and directed towards the interior of the loop, forming an internal ionic interaction with Arg32 of human TNF (Fig. 6). Modelling studies of human TNF with its receptors showed no direct involvement of residue 146 in receptor binding (Fu *et al.*, 1995). Amino acid 146 also belongs to the TNF-R75-specific region (Van Ostade *et al.*, 1994). These findings suggest that the orientation of the side chain of Glu146 might be important for the species specificity of receptor binding.

The loop region containing residues 68–75 is different in mTNF because mTNF lacks His73, which makes the loop in mTNF smaller than in human TNFs. This region, however, is not involved in receptor binding.

The loop region 21–26 is also different in mTNF and human TNFs. This is probably a result of packing. None of these residues plays a role in receptor binding.

Five amino acids have a conserved hydrogen bond within the trimer in mouse and human TNF: Tyr59 OH (*A*/*B*/*C*) with Val123 N (*C*/*A*/*B*), Tyr72 OH (*A*/*B*/*C*) with Pro113 O (*B*/*C*/*A*), Ser95 N (*A*/*B*/*C*) with Gly148 O (*B*/*C*/*A*), Tyr119 OH with Gly121 O (*C*/*A*/*B*) and Gly121 O (*A*/*B*/*C*) with Tyr151 OH (*B*/*C*/*A*). Gln61 NE2 from mTNF (*A*/*B*/*C*) makes a hydrogen bond with Ser95 O (*C*/*A*/*B*), while for Gln61 NE2 from human TNFs there is only a hydrogen bond between Gln61 NE2 (*B*/*C*) and Ser95 O (*A*/*B*). These conserved hydrogen bonds are all located in the groove between two adjacent monomers, with the exception of the hydrogen bond formed by amino acids 119 and 121, which is located in the trimeric channel.

The trimeric channel in mouse TNF is closely packed and is even narrower than in human TNF. After superposition of the trimers of mTNF and hTNF97, the rotation angle between corresponding monomers is 3.9° for subunit *A*, 1.4° for subunit *B* and 1.7° for subunit *C*. The channel narrowing calculated from these least-squares transformation matrices is 1.0, 0.5 and 0.6 Å at the top, centre and bottom, respectively. A similar superposition of the trimers of mTNF and 1TNF shows equivalent rotation angles and channel narrowing. This narrower trimeric channel indicates that the mTNF trimer with one 2-propanol and one Tris molecule in the trimeric channel might be more stable. However, crystal-packing effects cannot be excluded. Assuming that the channel narrowing can be attributed to the 2-propanol molecule locked in the hydrophobic region of the trimeric channel, we put 2-propanol forward as a lead compound for the design of modulators for the trimerization of TNF. This trimerization is necessary for biological activation of the TNF receptors. Blocking this trimerization will stop TNF from exerting its biological activity and could therefore be helpful in combating autoimmune diseases such as rheumatoid arthritis and Crohn's disease.

In conclusion, mTNF is the best refined of all known TNF structures. The overall architecture of mTNF and human TNFs is identical. The packing of the trimers, however, is different. Compared with human TNFs, the trimeric channel is smaller. The Glu side chain of residue 146 is rotated away by 180° from human TNFs and becomes available for receptor binding.

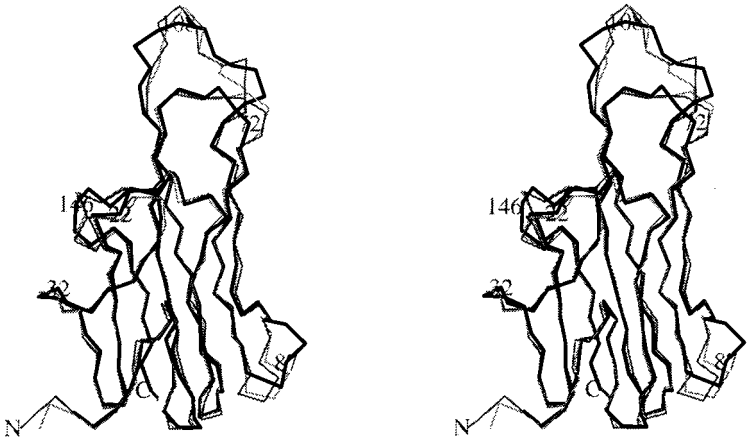

Figure 5
Stereoview of the C^{α} superposition of the monomers *B* of mTNF (black) and 1TNF (light grey) and hTNF97 (dark grey), showing the loop regions which are different for mouse and human TNFs.

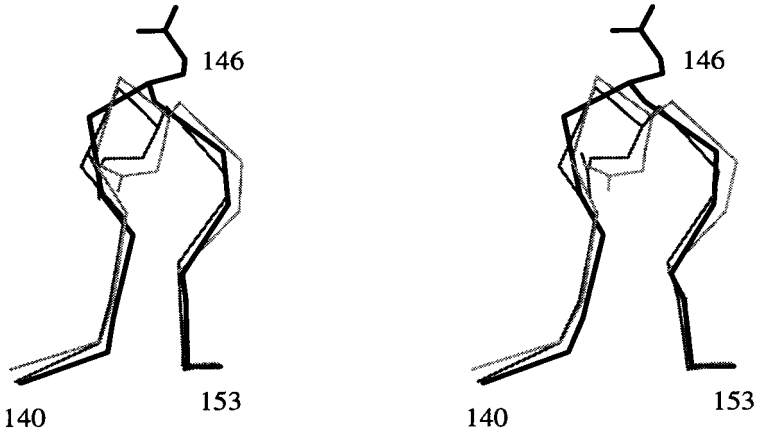

Figure 6
Stereoview of the superposition of Glu146 of mTNF (black) subunit *B* and 1TNF (light grey) and hTNF97 (dark grey) subunit *B*. The side chain of Glu146 of mTNF is rotated away by 180°. This figure is shown in the same orientation as Fig. 4.

We thank Professor I. Weber for sharing the coordinates of hTNF97 prior to publication. We thank the European Union for support of the work at EMBL Hamburg through the HCMP to Large Installations Project. HDB is a Postdoctoral Research Fellow of the National Fund for Scientific Research (Belgium).

References

Aggarwal, B. B. (1990). *Tumor Necrosis Factor: Structure, Function, Mechanism of Action, Role in Disease and Therapy*, edited by G. Bonavida & G. Granger, pp. 49–54. Basel: Karger.

Baeyens, K. J., De Bondt, H. L., Raeymaekers, A., De Ranter, C. J. & Fiers, W. (1997). *Acta Cryst.* D**53**, 329–330.

Banner, D. W., D'Arcy, A., Janes, W., Gentz, R., Schoenfeld, H.-J., Broger, C., Loetscher, H. & Lesslauer, W. (1993). *Cell*, **73**, 431–445.

Barbara, J. A. J., Smith, W. B., Gamble, J. R., Van Ostade, X., Vandenabeele, P., Tavernier, J., Fiers, W., Vadas, M. A. & Lopez, A. F. (1994). *EMBO J.* **13**, 843–850.

Brouckaert, P., Libert, C., Everaerdt, B. & Fiers, W. (1992). *Lymphokine Cytokine Res.* **11**, 193–196.

Brünger, A. T. (1990). *Acta Cryst.* A**46**, 46–57.

Brünger, A. T. (1992*a*). *X-PLOR Version* 3.1. *A System for X-ray Crystallography and NMR.* New Haven, Connecticut, USA.

Brünger, A. T. (1992*b*). *Nature (London)*, **355**, 472–474.

Brünger, A. T., Krukowski, A. & Erickson, J. (1990). *Acta Cryst.* A**46**, 585–593.

Brünger, A. T., Kuriyan, J. & Karplus, M. (1987). *Science*, **235**, 458–460.

Cha, S.-S., Kim, J.-S., Cho, H.-S., Shin, N.-K., Jeong, W., Shin, H.-C., Kim, Y. J., Hahn, J. H. & Oh, B.-H. (1998). *J. Biol. Chem.* **273**, 2153–2160.

Eck, M. J. & Sprang, S. R. (1989). *J. Biol. Chem.* **264**, 17595–17605.

Engh, R. A. & Huber, R. (1991). *Acta Cryst.* A**47**, 392–400.

Fiers, W. (1995). *Biologic Therapy of Cancer*, 2nd ed., edited by V. T. DeVita Jr, S. Hellman & S. A. Rosenberg, pp. 295–327. Philadelphia: Lippincott.
Fu, Z.-Q., Harrison, R. W., Reed, C., Wu, J., Xue, Y.-N., Chen, M.-J. & Weber, I. T. (1995). *Protein Eng.* **8**, 1233–1241.
Hutchinson, E. G. & Thornton, J. M. (1996). *Protein Sci.* **5**, 212–220.
Jiang, J.-S. & Brünger, A. T. (1994). *J. Mol. Biol.* **243**, 100–115.
Jones, E. Y., Stuart, D. I. & Walker, N. P. C. (1989). *Nature (London)*, **338**, 225–228.
Jones, T. A., Zhou, J. Y., Cowan, S. W. & Kjeldgaard, M. (1991). *Acta Cryst.* A**47**, 110–119.
Laskowski, R. A., MacArthur, M. W., Moss, D. S. & Thornton, J. M. (1993). *J. Appl. Cryst.* **26**, 283–291.
Luzzati, V. (1952). *Acta Cryst.* **5**, 802–807.
Otwinowski, Z. (1993). *Proceedings of the CCP4 Study Weekend. Data Collection and Processing*, edited by L. Sawyer, N. Isaacs & S. Bailey, pp. 56–62. Warrington: Daresbury Laboratory.
Porter, A. G. (1990). *FEMS Microbiol. Immunol.* **64**, 193–200.
Reed, C., Fu, Z.-Q., Wu, J., Xue, Y.-N., Harrison, R.W., Chen, M.-J. & Weber, I. T. (1997). *Protein Eng.* **10**, 1101–1107.
Vandenabeele, P., Declercq, W., Beyaert, R. & Fiers, W. (1995). *Trends Cell Biol.* **5**, 392–399.
Van Ostade, X., Tavernier, J. & Fiers, W. (1994). *Protein Eng.* **7**, 5–22.
Van Ostade, X., Tavernier, J., Prange, T. & Fiers, W. (1991). *EMBO J.* **10**, 827–836.
Van Ostade, X., Vandenabeele, P., Everaerdt, B., Loetscher, H., Geutz, R., Brockhaus, M., Lesslauer, W., Tavernier, J., Brouckaert, P. & Fiers, W. (1993). *Nature (London)*, **361**, 266–269.
Vassalli, P. (1992). *Annu. Rev. Immunol.* **10**, 411–452.
Yamagishi, J.-I., Kawashima, H., Matsuo, N., Ohue, M., Yamayoshi, M., Fukui, T., Kotani, H., Furuta, R., Nakano, & Yamada, M. (1990). *Protein Eng.* **3**, 713–719.
Zhang, X.-M., Weber, I. T. & Chen, M.-J. (1992). *J. Biol. Chem.* **267**, 24069–24075.